Microporous and Mesoporous Materials 152 (2012) 58–63

Contents lists available at SciVerse ScienceDirect

Microporous and Mesoporous Materials

journal homepage: www.elsevier.com/locate/micromeso

Bioactive TiO_2 ultrathin film with worm-like mesoporosity for controlled drug delivery

Chih-Shin Chao [a], Kun-Ho Liu [b], Wei-Lin Tung [a], San-Yuan Chen [a], Dean-Mo Liu [a,c,*], Yen-Po Chang [a,*]

[a] Department of Materials Science and Engineering, National Chiao Tung University, 1001 Ta-hsueh Rd., Hsinchu 300, Taiwan
[b] Advanced Delivery Technology Co. Ltd., No. 120-D, Zhonghua Rd., Hukou Township, Hsinchu 303, Taiwan
[c] Institute of Traditional Medicine, School of Medicine, National Yang-Ming University, PeiTou, 114 Taipei, Taiwan

ARTICLE INFO

Article history:
Received 1 September 2011
Received in revised form 30 November 2011
Accepted 2 December 2011
Available online 10 December 2011

Keywords:
Mesoporous TiO_2
Ultrathin film
Controlled drug release
Cytocompatibility
Bioactive coating

ABSTRACT

Ultrathin mesoporous TiO_2 coatings with a wormhole-like architecture were synthesized using evaporation-induced self-assembly method. The morphological and chemical structures of TiO_2 films were characterized using small-angle and large-angle X-ray diffraction, scanning electron microscopy (SEM), transmission electron microscopy (TEM) and Fourier transformed infrared spectrometry (FTIR). The films demonstrated a thickness of ~120 nm and open-porous nanostructure. By taking advantage of the tortuosity of the worm-like mesoporous architecture associated with the chemistry of the TiO_2 film, a sustained drug release using ibuprofen and vancomycin as model molecules from the film was determined. Besides, adhesion behavior of osteoblast cells, together with an in vitro apaptitic formation substantiated the cytocompatibility and bioactivity of the mesoporous TiO_2 films. Such combined bioactive and drug-releasing functions of the TiO_2 films with worm-like mesoporosity ensure an improved therapeutic performance for potential applications included orthopedics, dentistry, and drug delivery.

1. Introduction

Titanium exhibits desired mechanical properties such as moderate elasticity, high strength-to-weight ratio and biocompatibility. Hence, titanium and its oxidative derivatives, such as TiO_2, have long been employed for biomedical applications in the areas of dentistry, orthopedics and osteosynthesis. However, titanium-based implants with their surfaces have been realized not able to firmly attach to the host tissues due to fibrous capsule formed on titanium surface in vivo [1,2]. In order to avoid implant loosening and failure, the methods of coating bioactive thin films on implants have been developed, such as anodic oxidation [3], sol–gel technology [4,5], plasma spray [6], and sputtering [7]. Appropriate coatings are advantageous and even necessary for the acceptance and functioning of the implant. In several studies, TiO_2 thin film coatings was used to improve the hydrophilic properties of implants to favor osteoblast cell adhesion and enhanced the expressions of osteogenic genes [8,9]. Therefore, TiO_2 thin film coatings show a strong interfacial bonding between TiO_2 surface and living tissue [10]. In recent years, the coated implant can be viewed as a combinatory drug/medical device which represents an emerging new trend in nanotherapeutics. A combination of therapeutic drug and medical device can be integrated to increase the performance and life time of currently used implants and improve clinical compliance and life quality of patients [11]. On this base, either porosity or thickness of the resulting coating may consider critical as a drug reservoir for suitable therapeutic performance. Too thick coating such as several tens to hundred of micrometers of thickness has been declined in practice due to mechanical instability and potential adverse complications, such as inflammation caused by coating fragmentation after implantation [12–14]. On the other hand, coating with desired pore size or porosity has been highlighted and is expected to be tunable according to the therapeutic molecules to be carried and delivered.

Hence, it is technically and medically important to design an ultrathin porous coating capable of carrying and delivering drug with reasonably time period for improved therapeutic performance, especially for hard-tissue implants. Since the discovery of the MCM-type mesoporous materials [15], great attention has been focused on the synthesis and characterization of surfactant-templated mesoporous silica materials [16,17]. Due to the possibility of the strict control of their pore size, pore structure and surface properties, increasing interest has been directed to the exploration of mesoporous silica materials for drug delivery systems [18,19]. Furthermore, thin films of mesoporous oxide materials may offer more therapeutic opportunities for biomedical applications, particularly for implanted or invasive medical devices.

* Corresponding authors. Address: Department of Materials Science and Engineering, National Chiao Tung University, 1001 Ta-hsueh Rd., Hsinchu 300, Taiwan, ROC. Tel.: +886 3 5712121#55391; fax: +886 3 5724727.
E-mail addresses: deanmo_liu@yahoo.ca (D.-M. Liu), ypchang1021@gmail.com (Y.-P. Chang).

1387-1811/$ - see front matter © 2011 Elsevier Inc. All rights reserved.
doi:10.1016/j.micromeso.2011.12.006

In this study, evaporation-induced self-assembly (EISA) method was used to synthesize mesoporous TiO_2 ultrathin films. Taking advantages of the simplicity of synthetic process, mesoporous TiO_2 thin films can be used to modify the surface and improved biofunctionality of medical implants. In the meantime, we also employ those mesopores of TiO_2 thin films to carry ibuprofen and vancomycin followed by a controlled release of the drug, for therapeutic purpose. Cytocompatibility and bioactivity of the resulting mesoporous TiO_2 ultrathin film were evaluated in vitro using osteoblast adhesion test and apatitic formation in the presence of acellular simulated body fluid, respectively.

2. Experiment

2.1. Preparation of the mesoporous TiO_2 ultrathin films

Titanium tetraisopropoxide (TTIP, 98%, ACROS), acetyl acetone (AcAc), and 2-propanol was stirring as precursor solution. The surfactant block copolymer P123 [$HO(CH_2CH_2O)_{20}(CH_2CH(CH_3)O)_{70}(CH_2CH_2O)_{20}H$, Aldrich] was slowly added to the precursor solution. The obtained solution was hydrolyzed at a pH 1.2 condition. The molar ratio of P123/TTIP/AcAc/IPA was 0.03/1/0.5/35. The mixture was stirred for 3 h and spin-coated on silicon (100) or glass substrate at 2000 rpm—30 s. Finally, the spin coated films were calcined at 450 °C for 4 h.

2.2. Characterization of the mesoporous TiO_2 ultrathin films

The resulting ultrathin films on silicon substrate were characterized using powder X-ray diffraction (PXRD) measurements (MAC Science MXP18AHF XRD, with Cu Kα radiation source, λ = 1.5418 Å). TEM micrographs, electron diffraction patterns were recorded by a JEOL JEM-2100F electron microscope equipped with an Oxford energy-dispersive spectrometer (EDS) analysis system. For the cross-sectional TEM characterization, the calcined sample was first cleaved into small pieces of ~2 mm × 3 mm, then pairs of such pieces were glued to each other through face-to-face contact. The glued stacks were mechanically ground and polished into wedge shapes, followed by chemical polishing with Rodel NALCO 2354 CMP fluid. Fourier transformed infrared spectroscopy (ATR-FTIR) spectra were recorded on a spectrometer (Bomem DA8.3, Canada) with a KBr plate. The FTIR spectra were taken with a resolution of 2 cm^{-1} in the range of 4000–450 cm^{-1}.

2.3. Loading and release behavior of IBU

First, the films (2 × 2 cm^2) were impregnated with a 2 ml of ibuprofen solution (IBU) in ethanol (5 mg/ml, 10 mg/ml, 40 mg/ml) for a time period of 24 h and were dried at 50 °C. Then, the films were washed with 10 ml of phosphate buffer saline (PBS) to remove the excess IBU resided along the surface region. The amount of drug encapsulated in the mesoporous TiO_2 film was then calculated by the initial amount of drug subtracting the drug left in the supernatant. Encapsulation efficiency (EE) of drug was obtained as described below

$$\text{EE } (\%) = (A - B)/A \times 100$$

where A is the total amount of the drug and B is the amount of drug remaining in the supernatant. In order to compare the drug loading and release behavior of IBU and VAN, the films (2 × 2 cm^2) were impregnated with 2 ml of (1) IBU in ethanol and (2) vancomycin (VAN) in DI water of 10 mg/ml concentration, respectively, for 24-h period, followed by washing with 10 ml PBS to remove surface drugs and dried at 50 °C. For drug release evaluation, the drug-loaded films were immersed in a PBS solution and concentration of released IBU or VAN was measured by UV/Vis spectrophotometer at wavelength of 254 nm and 282 nm, respectively.

2.4. Cell culture test of the mesoporous TiO_2 ultrathin films

The mouse bone marrow osteoblastic cells, 7F2, were cultured in medium containing 90% alpha minimum essential medium with 2 mM L-glutamine and 1 mM sodium pyruvate without ribonucleosides and deoxyribonucleosides, 10% fetal bovine serum and maintained in humidified atmosphere with 5% CO_2 at 37 °C. Then, the cells seeded with a density of 5 × 10^3 cells/cm^2 on different specimen surfaces for cytocompatibility evaluation.

After 48 h of incubation, cells were fixed in 3.7% formaldehyde and permeabilization was performed with 0.1% trixon-100 in PBS. 7F2 cells were washed with PBS and then stained with Rhodamine–Phalloidin (1 μg/ml) at 37 °C for 1 h. Then the cell morphology was investigated by fluorescent microscope (×400, eclipse, TE2000-U, Nikon). Three samples of each group, i.e., control, TiO_2 film without calcinations, TiO_2 film with calcinations, were prepared for statistical analysis and five randomly selected images from one sample substrate were captured and calculated. The cell number was collectively measured and averaged for those three samples and presented as mean ± SD.

2.5. Bioactivity of the mesoporous TiO_2 ultrathin films

The mesoporous TiO_2 ultrathin films (1 × 1 cm^2) were immersed in 10 ml SBF with ion concentrations (Na^+ 213.0, K^+ 7.5, Ca^{2+} 3.8, Mg^{2+} 2.3, Cl^- 221.7, HCO_3^- 6.3, HPO_4^{3-} 1.5, SO_4^{2-} 0.8 mM), nearly equal to those in human blood plasma, at 36.5 °C and contained in a polystyrene bottle. The SBF was prepared by dissolving reagent grade chemicals of $CaCl_2$, $K_2HPO_4{\cdot}3H_2O$, KCl, NaCl, $MgCl_2{\cdot}6H_2O$, $NaHCO_3$, and Na_2SO_4 in DI water and buffered at pH 7.4 using *tris*(hydroxymethyl)-aminomethane ($(CH_2OH)_3CNH_2$) and 1 M HCl at 36.5 °C. After a given immersion period, the films were removed from the SBF, gently washed with DI water, and dried at 40 °C. The surfaces of the immersed films were analyzed by SEM (JEOL 6500) and XRD (Shimadz XRD-6000, λ = 1.541 Å).

3. Results and discussion

3.1. Characteristics of mesoporous TiO_2 ultrathin film

To obtain mesoporous TiO_2 ultrathin film, poly(alkylene oxide) block polymer (designated $EO_{20}PO_{70}EO_{20}$; Pluronic P123) was used as a soft template. A sol–gel process was employed by hydrolyzing organometallic titanium isopropoxide in the presence of P123 templates. After condensation, the mesoporous structure of TiO_2 film was evolved by removing the template at 450 °C for 6 h in air. The calcined TiO_2 film was examined using large-angle XRD

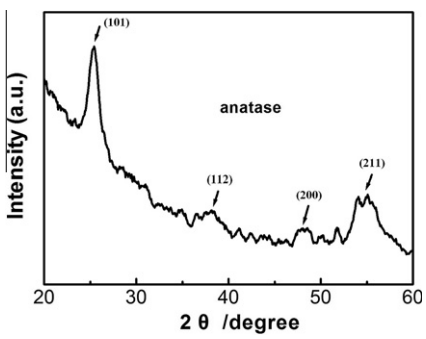

Fig. 1. Large-angle XRD pattern of the mesoporous TiO_2 ultrathin film.

(LA-XRD), where the resulting pattern, Fig. 1, shows four characteristic peaks of the basal reflections of (101), (112), (200), and (211) planes at $2\theta = 25.4°$, 38.3°, 48.1°, 55°, respectively, corresponding to the tetragonal crystalline TiO_2 phase (JCPDS No. 21-1272). Intensive and sharp diffraction peaks indicated highly crystalline TiO_2 frameworks with space group I41/amd (141). Fig. 2 shows the small-angle X-ray diffraction (SA-XRD) patterns of the as-synthesized and calcined mesoporous TiO_2 films. In Fig. 2(a), a characteristic reflection of the p6mm hexagonal structure at $2\theta = 0.96°$ and $2\theta = 1.66°$ is observed and the corresponding spacing ($d_{spacing}$) is indexed with $d_{100} = 9.2$ nm and $d_{110} = 5.32$ nm, respectively. The hexagonal unit cell parameter (a_o) of 10.6 nm was calculated from assuming a (100) reflection of the hexagonal array of mesoporous TiO_2 film. Those aforementioned results indicate that the as-synthesized mesoporous TiO_2 film exhibits highly-ordered arrays. After calcination, Fig. 2(b) shows a single broad diffraction peaks at $2\theta = 1.2°$ with the corresponding spacing ($d_{spacing}$) indexed with $d_{100} = 7.36$ nm, being suggestive of mesostructural order [20].

Fig. 3 shows the cross-sectional TEM images of the calcined mesoporous TiO_2 film, whereas a thickness of ~126 nm with uniform worm-like mesoporous structure can be found. The thickness of the solid framework was ca. 5–8 nm which is thicker than that of pore size (ca. 4 nm). It is well-known that high-temperature calcination causes severe shrinkage of TiO_2 film structure [21,22], the structure mesoporous TiO_2 film is therefore expected to be disturbed while calcining at high temperatures and in this case, as large as ~20% of shrinkage was measured. However, experimental observation indicated structural integrity reminded intact for the mesoporous TiO_2 film, where a thicker wall of the mesoporous film is expected to keep the structure from collapsing during calcination [23]. In addition, the uneven framework is considered to result in the broad diffraction peak of SA-XRD pattern. The worm-like channels that are more or less regular in diameter were packed in random forming a three dimensional mesoporous structure, which may also contribute to the single broad peak observed over the low-angle region. It exhibits mesoporous TiO_2 framework with well-crystalline nanostructure, corresponding to the intensive diffraction peak for the LA-XRD pattern, as the high resolution TEM image given in the inset of Fig. 3.

Both the XRD and TEM analyses confirmed the formation of worm-like mesoporous structure of the TiO_2 film coating through the use of sol–gel synthesis, associated with the presence of a molecular template. The open pore structure of the resulting TiO_2 film permits its potential capability to carry pharmaceutical substances for improved therapeutic purposes. The worm-like structure developed throughout the mesoporous ultrathin film was believed to be a result due to the molecular assembly of the soft template upon rigid framework development upon the synthesis, which also provides a highly tortuous path for a potential sustained delivery of therapeutic molecules.

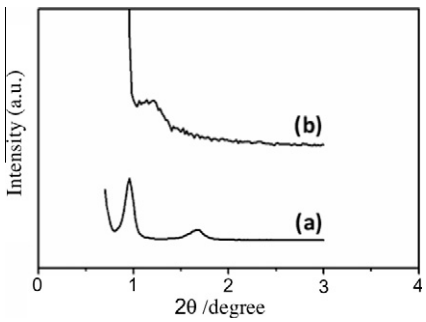

Fig. 2. Small-angle XRD pattern of the mesoporous TiO_2 ultrathin film (a) before and (b) after calcination.

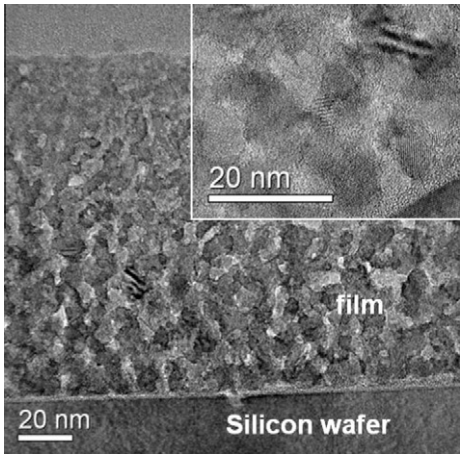

Fig. 3. TEM image of the mesoporous TiO_2 ultrathin film after calcination.

3.2. Drug loading and release behavior from mesoporous TiO_2 ultrathin film

Ibuprofen (IBU), an anti-inflammatory drug, was used as model molecule to demonstrate the encapsulation and eluting behavior of the mesoporous TiO_2 film. From the absorbance FTIR spectra, the mesoporous TiO_2 ultrathin film (Fig. 4(a)) shows characteristic bands of TiO_2: the bands around 3230 and 1620 cm^{-1} are due to the OH stretching vibration and OH deformation vibration, respectively, which can be attributed to the surface-adsorbed H_2O and hydroxide group (–OH) of TiO_2 [24]. The broad band at 450–900 cm^{-1} can be ascribed to the vibration of Ti–O bond in TiO_2 [25]. In addition, pure IBU shows a strong carboxyl band at 1730 cm^{-1}, which corresponds to the carboxyl group (C=O), as shown in Fig. 4(c). The absorption appearing around 1430 and 1250 cm^{-1} corresponds to CO asymmetric vibration. After loading of IBU, Fig. 4(b), it shows additional peaks at 2970–2880 cm^{-1} assigned to the symmetric and asymmetric stretching vibrations of $-CH_x$ groups, due to the IBU alkyl chain. In addition, the disappearance of a strong carboxyl band at 1730 cm^{-1}; instead, a new peak at 1550 cm^{-1} appeared which may be attributed to the asymmetric stretching vibration of COO^-, since carboxylic acid salts exhibit a strong characteristic COO^- asymmetric stretching band in the range of 1650–1550 cm^{-1} [26]. This observation indicated

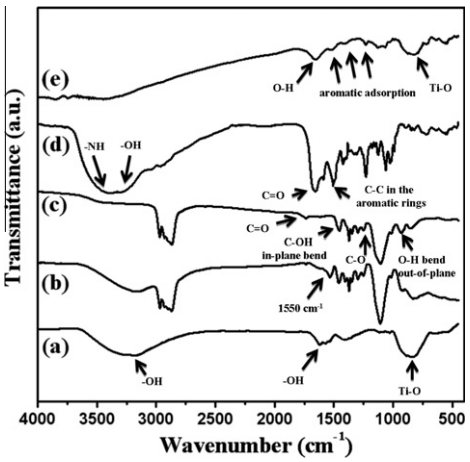

Fig. 4. FTIR spectra of (a) the mesoporous TiO_2 ultrathin film, (b) the IBU loaded mesoporous TiO_2 ultrathin film, (c) pure IBU, (d) pure VAN, and (e) the VAN loaded mesoporous TiO_2 ultrathin film.

a deprotonation of the IBU molecule when it was interacted with the mesoporous TiO_2 film, suggesting a strong chemical affinity between the IBU and the ultrathin film. Such an interaction, according to the spectral analysis aforementioned, is likely a hydrogen bonding between the carboxyl group of IBU and hydroxyl group of the TiO_2 film. In addition, the FT-IR spectrum of vancomycin shows in Fig. 4(d). Additional well-pronounced bands in the range from 1700 to 1000 cm^{-1} and from 3600 to 2800 cm^{-1} are the characteristic bands of vancomycin. For instance, a strong carboxyl band at 1680 cm^{-1}, characteristic band of a C–C mode of vibration in the aromatic rings at 1493 cm^{-1}, and N–H and/or O–H stretching vibration at 3400–3200 cm^{-1}, respectively. While loading with vancomycin (VAN), FT-IR spectrum, Fig. 4(e), depicts characteristic bands at 3400 cm^{-1} and 1650 cm^{-1} designated the stretching and bending vibrations of the O–H bond. Compared to the FT-IR spectra of TiO_2, three new bands were observed for TiO_2 after incorporation of VAN at 1510 cm^{-1}, 1420 cm^{-1}, and 1230 cm^{-1}, which were attributed to aromatic adsorption from the VAN molecule. It is indicated that the surface of the mesoporous TiO_2 film was covered with sufficient amount of vancomycin.

When different concentrations of IBU (5 mg/ml, 10 mg/ml, and 40 mg/ml) were incorporated in the mesoporous TiO_2 film, a drug encapsulation efficiency of 10%, 18%, and 5%, respectively, was observed. With the increase of IBU solution, a saturated drug payload of ca. 2 mg/ml was observed. Fig. 5 also indicates a slower release of IBU from the mesoporous film with the higher drug payload (immersed in 10 or 40 mg/ml) than that from the film with lower drug payload (i.e., in the case of 5 mg/ml). For the latter, IBU was depleted in about 10 h, whilst longer release profile of 30 h was achieved for the higher drug-loaded films. The slower release profile suggested that the release of IBU was effectively inhibited upon diffusion outward the TiO_2 film. Such a slower diffusion is believed to be related with tortuous porosity of the films where the IBU was loaded into deeper regions of the pore structure while impregnating with the high-concentrated IBU solution. Furthermore, as more drug molecules encapsulated in the mesoporous structure of the TiO_2 film, limited space may also restrict IBU diffusion, rendering a slower release profile, as evidenced in Fig. 5.

To further illustrate the size effect of the drug molecule on a subsequent release behavior from the mesoporous TiO_2 film, vancomycin was employed, which has a larger, by a factor of ca. 14 times, molecule size of $3.2 \times 2.2\ nm^2$ [27], compared with IBU, $\sim 1 \times 0.5\ nm^2$, and has a dimension closed to the pore size of the mesoporous TiO_2 film, as illustrated in Fig. 6(a) and (b). While impregnation with drug solution of 10 mg/ml concentration, VAN reached much lower drug payload of 0.75 mg/ml and showed faster release profile than that of IBU, Fig. 6(c), where ~95% VAN released in about 10 h and as high as 50% being burst released, whilst ~80% for the IBU over a 10 h period. Larger molecule size experiences more difficult in drug loading inside the pores, and this

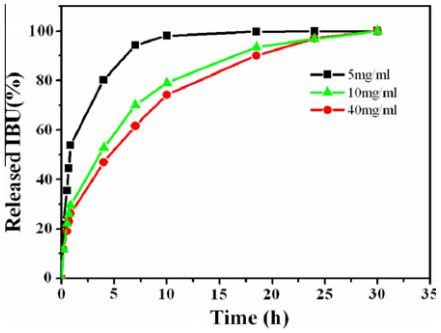

Fig. 5. Mean cumulative ibuprofen release behavior from the mesoporous TiO_2 ultrathin film with different immersed concentration.

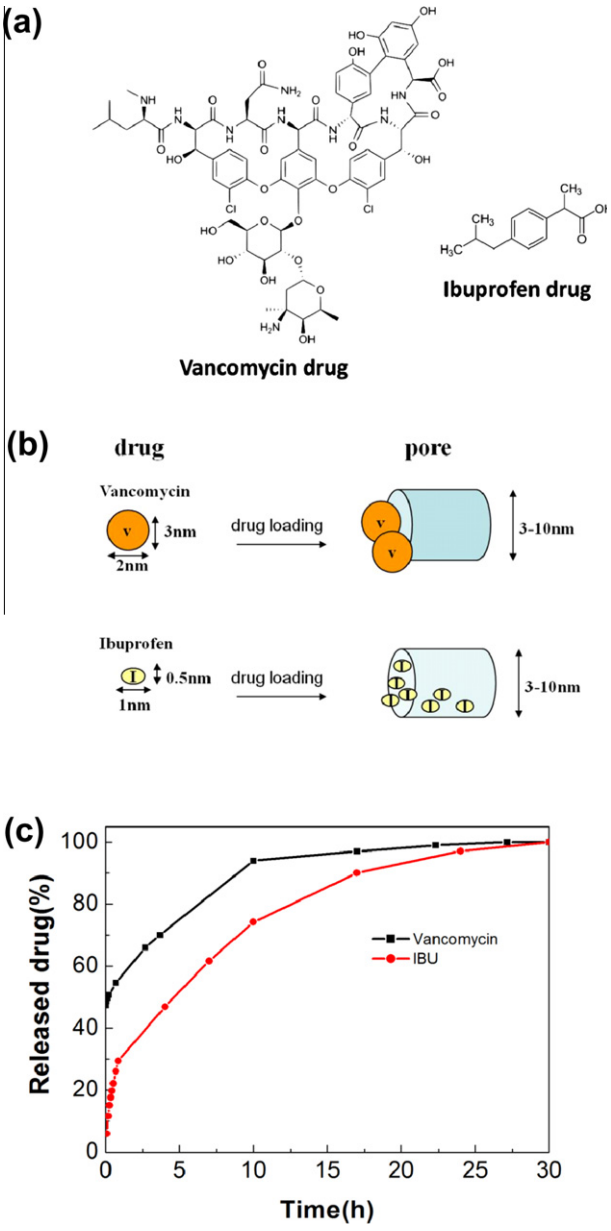

Fig. 6. The molecular structure of ibuprofen and vancomycin drugs (a), the illustration of drug loading method for various molecular size (b) and those drugs delivery profile during 30 h (c).

renders more surface-bounded drug and less drug resided within mesopores, giving rise to an early-phase burst, by 50% and a higher release rate within the first hour. In order to further understand the release behavior, diffusion exponent n was determined by the use of Power Law [28].

$$M_t/M_0 = kt^n, (M_t/M_0 \leqq 0.6)$$

where M_t is the amount of drug released at time t, M_0 is the amount of drug loaded, k is a rate constant and n is the diffusion exponent related to the diffusion mechanism. Herein, the diffusion exponent n and constant K calculated from the drug release profiles are 0.08, 0.48 and 33.2, 4.01 for VAN and IBU, respectively (R^2 = 0.99, 0.97 for VAN and IBU, respectively). There are three types of release profiles can be categorized. As the diffusion exponent n is closed to zero, the drug release rate remains constant until the exhaust of drug. The second common type of release kinetics is first-order release or diffusion-controlled release when n is closed to 0.5. The release

rate is proportional to the mass of drug contained within the device. It means the release rate declines exponentially with time, approaching a release rate of zero as the device approaches exhaustion. When the n is closed to one, swelling-controlled release kinetics is dominated. From the results, the diffusion exponent *n* of VAN closed to zero corresponds to a zero-order release kinetic while the diffusion exponent n of IBU closed to 0.5 showed Fickian diffusion kinetics. Zero-order release kinetic of VAN suggested a time-independent release that may be the cause of larger molecules tending to aggregate on the surface of TiO_2 films. On the other hand, IBU showed a diffusion-controlled release behavior which indicated the release rate of IBU molecules from TiO_2 film determined by the diffusion rate of molecules. Hence, it can be explained that smaller IBU molecules showed slower release rate than larger VAN molecules. Besides, from FTIR analysis aforementioned, it is reasonably to believe that both the pore size and chemical interaction between the drug molecule and TiO_2 surface play critical role in dominating the resulting release kinetics. Although it is hard to give a clear-cut of the released amount of the drugs that dominated by specific releasing mechanism, the interplay between these factors will depend on the relative amount of drug adsorbed onto and encapsulated into the porosity structure of the TiO_2 film. In general, this comparison suggests the worm-like nanostructure of the ultrathin film coating imparting considerable amount of porosity for drug load and in the meantime, increased the length of pathway for drug diffusion. Both contributions, associated with the chemical affinity, allow drug elution for time duration of 30 h over such an ultrathin coating. However, extended release with a controllable dosing quantity can be further designed, albeit not the main focus of this preliminary investigation, upon nanostructural optimization included coating thickness, porosity, and pore size through the use of soft-template synthesis for specific biomedical practices.

3.3. Cell culture of mesoporous TiO_2 film

The cellular behavior on the mesoporous TiO_2 film was examined by culturing murine osteoblast cells (7F2) on coated surfaces. Fig. 7 shows the cell adhesion and spreading on the mesoporous TiO_2 film with red fluorescent action skeleton by fluorescent microscopy. Osteoblast cells were seeded on the surface with three different morphological structures: mesoporous TiO_2 film before (Fig. 7(b)) and after calcination (Fig. 7(c)), and glass substrate (Fig. 7(a)) as control. All surfaces favored the adhesion and growth of 7F2 murine osteoblast cells, with no sign of cytotoxicity was detected. For optical microscopic observation of the cell morphology and growth condition, which was shown ~60 percent confluency during the tested time, and it would be clear and easy to observe and calculate under such seeding density. After 48 h of cultivation, cell seeded on calcined mesoporous TiO_2 film proliferated to a greater extent than non-calcined film and control group. After 6 h of incubation with calcined mesoporous TiO_2 surfaces, cells remained round shape. After 48 h, cell morphology was still intact in structure and most cells homogeneously spreaded and flattened on the surface. The morphology of 7F2 cells on non-calcined and glass surfaces were similar, however, the number of cells adhered to non-calcined surfaces was less than on the glass control, as displayed in Fig. 7(d), where for the former, residual solvent left within the non-calcined film may exert adverse effect on cell survival, suggesting the solid phase of the non-calcined film together with the templating surfactant are unlikely biocompatible to the cells. Compare with the control group and non-calcined film, 7F2 cells adhered much better and even supported and enhanced cell proliferation on the calcined mesoporous TiO_2 film.

3.4. Bioactivity of mesoporous TiO_2 ultrathin film

An easy and well-accepted method for estimate of bioactivity of a given surface in vitro is to examine whether the surface is able to induce the formation of apatitic (hydroxyl apatite) layer when soaked in a simulated body fluid (SBF) [29,30]. As an indication of bioactivity, the formation of an apatite layer on the implant surface in vitro was also observed in in vivo experiments and can be translated for the implants to form chemical bonding with living bone. TiO_2 has been reported to be bioactive as hard tissue implants, introduction of porosity turns to be critical in enhancing activity for a TiO_2 coating because the rough and porous surface can enlarge the area for cell attachment and spreading [31].

The formation of a bone-like apatite layer on a bioactive ceramics can be reproduced in an acellular simulated body fluid (SBF) with ion concentrations nearly equal to those of human

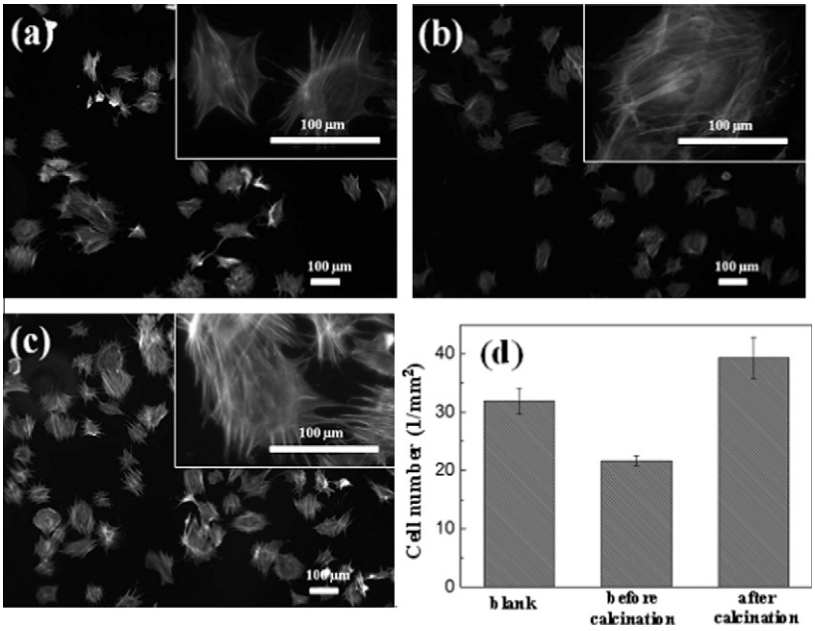

Fig. 7. Microscopic images (a–c) and cell number calculation (d) of osteoblastic cell incubated for 48 h on the different substrate (glass as control (a), TiO_2 ultrathin film for before (b) or after calcination (c)). For cell counting, the results were averaged and presented as mean ± SD, and analyzed by Student's *t*-test (*p* value <0.05).

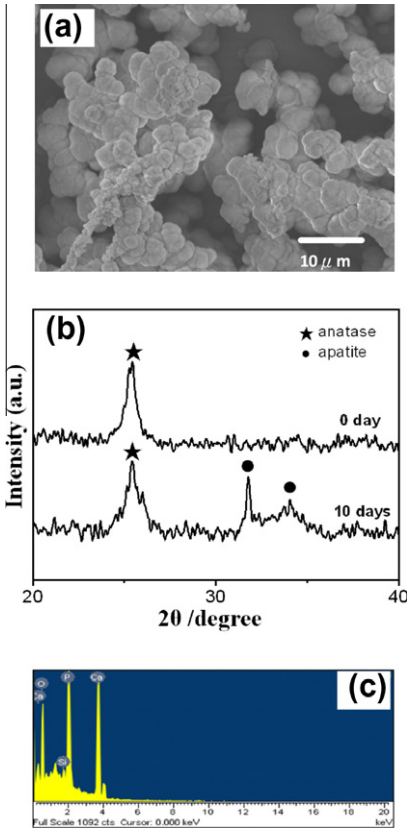

Fig. 8. (a) SEM, (b) LA-XRD and, (c) EDS analysis of the calcined mesoporous TiO_2 ultrathin film soaked in SBF for 10 days.

Table 1
Composition of calcium phosphate on mesoporous TiO_2 thin films soaked in SBF for 10 days.

Ten days after immersion in SBF	Contents of Ca atomic (%)	Contents of P atomic (%)
TiO_2 thin film before calcination	14.7	11.29
TiO_2 thin film after calcination	18.36	12.68

blood plasma. Fig. 8(a) shows the SEM micrographs of the calcined-mesoporous TiO_2 film soaked in SBF for 10 days. The characteristic apatite globular crystals are clearly visible, as shown in Fig. 8(b). Therefore, EDS analysis, Fig. 8(c) ensures that the surface layer observed in Fig. 8(a) is mainly composed of calcium phosphate (see Table 1). The crystal size of the apatite layer for 10 days incubation was about 1–3 μm and the Ca/P atomic ratio of bone-like apatite was 1.45, which is a typical Ca-deficient apatite, as generally observed in the literature reports. Such as that observed by Milella and coworkers on a titania gel, who suggested the apatite layer formation is virtually a result of that Ti–OH groups along the TiO_2 surface, causing apatite nucleation [32]. The hydroxyl groups favored reaction with Ca ions from the SBF, followed a subsequent deposition of phosphate groups to form apatite crystallite. Therefore, it suggested that the mesoporous TiO_2 ultrathin film prepared in the work is bioactive, and its worm-like nanostructure along the layer structure multi-functionalized the coating capable of delivering therapeutic drugs for biomedical purpose.

4. Conclusion

A facile method was employed to synthesize mesoporous structure of TiO_2 ultrathin films. LA-XRD, SA-XRD, and TEM images showed the formation of worm-like mesoporous structure TiO_2 framework with crystalline phase. The worm-like structure provides a tortuous path for therapeutic molecules to load and diffuse for drug release purpose. FTIR demonstrated that an interaction of the IBU molecule with the mesoporous TiO_2 film, suggesting a good chemical affinity between the IBU and the ultrathin film. Both the chemical affinity and mesoporosity dominate the resulting release profiles for both IBU and VAN molecules. The osteoblast adhesion and hydroxyl apaptite deposition confirmed excellent cytocompatibility and bioactive properties of the mesoporous TiO_2 films. Above results suggested that the mesoporous TiO_2 ultrathin film prepared in the work is bioactive, and its worm-like nanostructure, associated with surface chemistry, imparting a capability of simultaneous delivery of drugs for therapeutic purpose upon application.

Acknowledgements

This work was financially supported by the National Science Council of the Republic of China, Taiwan, under contracts 99-2221-E-009-070-MY3 and NSC-2113-M-009-027-MY2. This work is also supported by "Aim for the Top University Plan" of the National Chiao Tung University and Ministry of Education, Taiwan, ROC.

References

[1] A.A. Campbell, Mater. Today 11 (2003) 26–30.
[2] P.I. Brånemark, J. Prosthet. Dent. 50 (1983) 399–410.
[3] B. Yang, M. Uchida, H.M. Kim, X. Zhang, T. Kokubo, Biomaterials 25 (2004) 1003–1010.
[4] T. Peltola, M. Jokinen, H. Rahiala, M. Pätsi, J. Heikkilä, I. Kangasniemi, A. Yli-Urpo, J. Biomed. Mater. Res. 51 (2000) 200–208.
[5] S. Areva, V. Ääritalo, S. Tuusa, M. Jokinen, M. Lindén, T. Peltola, J. Mater. Sci. Mater. Med. 18 (2007) 1633–1642.
[6] C.M. Vallecillo, O.M.N. Romero, G.M.V. Olmedo, B.C. Reyes, R.C. Zorrilla, J. Oral. Implantol. 33 (2007) 59–68.
[7] U. Brohede, S. Zhao, F. Lindberg, A. Mihranyan, J. Forsgren, M. Strømme, E. Håkan, Appl. Surf. Sci. 255 (2009) 7723–7728.
[8] Z. Zhang, J. Sun, H. Hu, Q. Wang, X. Liu, J. Biomed. Mater. Res. 97 (2011) 224–234.
[9] F. Likibi, B. Jiang, J. Mater. Res. 23 (2008) 3222–3228.
[10] M. Ueda, H. Sai, M. Ikeda, M. Ogawa, Mater. Sci. Forum 654–656 (2010) 2257–2260.
[11] D. Triggle, J. Med. Princ. Pract. 16 (2007) 1–14.
[12] C.A. Grimes, J. Mater. Chem. 17 (2007) 1451–1457.
[13] K.A. Gross, W. Walsh, E. Swarts, J. Therm. Spray Technol. 13 (2004) 190–199.
[14] B. León, J.A. Jansen, Thin Calcium Phosphate Coatings for Medical Implants, Springer Verlag, New York, 2009.
[15] C.T. Kresge, M.E. Leonowicz, W.J. Roth, J.C. Vartuli, J.S. Beck, Nature 359 (1992) 710–712.
[16] P. Yang, D. Zhao, B.F. Chmelka, G.D. Stucky, Chem. Mater. 10 (1998) 2033.
[17] Q. Huo, D.I. Margolese, U. Ciesla, P. Feng, T.E. Gier, P. Sieger, R. Leon, P.M. Petroff, F. Schüth, G.D. Stucky, Nature 368 (1994) 317–321.
[18] M. Suh, H.J. Lee, J.Y. Park, U.H. Lee, Y.U. Kwon, D.J. Kim, ChemPhysChem 9 (2008) 1402–1408.
[19] H. Hata, S. Saeki, T. Kimura, Y. Sugahara, K. Kuroda, Chem. Mater. 11 (1999) 1110–1119.
[20] J.C. Yu, L.Z. Zhang, J.G. Yu, New J. Chem. 26 (2002) 416–420.
[21] E. Crepaldi, G.J. Soler-Illia, D.A.A. Grosso, D. Albouy, P.A. Amenitsch, C. Sanchez, Stud. Surf. Sci. Catal. 141 (2002) 235–242.
[22] J.C. Yu, L. Zhang, Z. Zheng, J. Zhao, Chem. Mater. 15 (2003) 2280–2286.
[23] H. Li, W. Shen, J. Shi, L. Xiong, J. Liang, M. Ruan, J. Mater. Res. 21 (2006) 380–385.
[24] Z. Ding, G.Q. Lu, P.F. Greenfield, J. Phys. Chem. B 104 (2000) 4815–4820.
[25] B. Tian, F. Chen, J. Zhang, M. Anpo, J. Colloid Interf. Sci. 303 (2006) 142–148.
[26] G. Socrates, Infrared Characteristic Group Frequencies: Tables and Charts, Wiley, New York, 1994.
[27] T. Lopez, J. Navarrete, R. Conde, J.A. Ascencio, J. Manjarrez, R.D. Gonzalez, J. Biomed. Mater. Res. 78 (2006) 441–448.
[28] N.A. Peppas, Pharm. Acta Helv. 60 (1985) 110–111.
[29] M. Uchida, H.M. Kim, T. Kokubo, S. Fujibayashi, T. Nakamura, J. Biomed. Mater. Res. 64 (2003) 164–170.
[30] K. Prashantha, B.J. Rashmi, T.V. Venkatesha, J.H. Lee, Spectrochim. Acta A 65 (2006) 340–344.
[31] E. Gultepe, D. Nagesha, S. Sridhar, M. Amiji, Adv. Drug Deliv. Rev. 62 (2010) 305–315.
[32] C. Massaro, M.A. Baker, F. Cosentino, P.A. Ramires, S. Klose, E. Milella, J. Biomed. Mater. Res. 58 (2001) 651–657.